Photon-Counting Gamma Camera Based on an Electron-Multiplying CCD

Gerralt A. de Vree, *Student Member, IEEE*, Albert H. Westra, Ian Moody, Frans van der Have, *Student Member, IEEE*, Kees M. Ligtvoet, and Freek J. Beekman, *Senior Member, IEEE*

***Abstract*—We have developed a compact ultra-high-resolution gamma camera (UGC), based on an electron-multiplying charge-coupled device (EMCCD) coupled to a columnar CsI(Tl) scintillator. The EMCCD is suitable for photon-counting gamma-camera imaging, since it has an extremely low readout noise, even at high frame rates (<1 electron/pixel at 50 images/s or 11 Mpixel/s). The high frame rate prevents overlapping of scintillation events and reduces the accumulation of dark current noise. In this paper, we describe the drive- and readout electronics of the EMCCD, the image processing hardware and software, and the first ultra-high-resolution gamma-ray images obtained with the UGC. A digital signal processor (DSP) facilitates real-time frame analysis, comprising photon counting and energy discrimination, and reduces the data stream from 162 kB per frame to 8 B per detected scintillation event (i.e., for a typical application in multipinhole single photon emission computed tomography (SPECT) a data reduction from 28 GB/h by a factor of 20 000 to 1.4 MB/h). Such a reduced data stream is needed for applications that require the use of a large number of gamma cameras simultaneously. The image processing hardware that we describe allows the images from the EMCCD to be processed in real-time, at a rate of 50 images per second. First gamma-camera images with a spatial resolution as good as 60 μm full-width of half-maximum (FWHM) are shown. The prototype UGC allows for photon counting without the need for an image intensifier and has energy discriminating capabilities.**

***Index Terms*—Charge-coupled device (CCD), digital signal processor (DSP), electron-multiplying charge-coupled device (EMCCD), gamma camera, molecular imaging, photon-counting, readout electronics, single photon emission computed tomography (SPECT).**

I. Introduction

COMPACT high-resolution gamma cameras are very useful in applications like small animal pinhole single photon emission computed tomography (SPECT) imaging. With small detectors one can place many pinhole cameras around the object of investigation, resulting in a high counting sensitivity [1]–[9]. Other applications of compact gamma cameras include planar gamma camera imaging [10]–[12], radiation monitoring (e.g., [13]), tumor surgery [14], and autoradiography [15].

In recent years different high-resolution detectors have been proposed. For example semiconductor detectors based on CdZnTe have been developed by several groups for nuclear medicine and X-ray astronomy applications (see for example [16] and [17]). Examples of two-dimensional (2-D) and three-dimensional readout of the CdZnTe are the MediPix2 Chip [18] and methods like those proposed by He *et al.* [19], respectively.

Another option to obtain high spatial resolution is the use of a detector based on micro-columnar scintillation crystals. The columnar structure prevents resolution loss due to light spreading in the scintillator. As an example, thallium-doped CsI has high-Z components, a high density, and an excellent scintillation light yield, which makes it an excellent detector material for gamma-ray detection. These particular crystals can be grown in tiny columnar structures, yielding a high spatial resolution when read out with a charge-coupled device (CCD) (e.g., [20]). The potential of CCDs to read out crystals for photon-counting applications is growing, since the quantum efficiency and noise properties of CCDs are steadily improving. Methods are foreseen for eliminating depth-of-interaction problems in scintillation pinhole gamma cameras based on columnar crystals [8].

One can distinguish two classes of scintillation gamma (or X-ray) cameras. One is the integrating camera in which each pixel gives a signal that is more or less proportional to the total amount of light received from scintillations observed during a fairly long period. As a result one loses information about the amount of scintillation light that each individual gamma quantum contributes to a (CCD) pixel. Also the center of gravity of the individual scintillation events can no longer be determined, which reduces possibilities to optimize spatial resolution. A second class consists of photon-counting scintillation gamma cameras. Photon-counting scintillation gamma cameras often have the potential to analyze properties of each light flash and to discriminate whether a light flash should be rejected on the basis of the amount and spatial distribution of the scintillation light observed. Photon counting as defined in the present paper involves that positions and intensities of individual flashes are estimated in CCD-frames. The estimated locations of flashes with a certain range of intensities are then used to form a gamma-camera image. The intensity estimate can be used for energy discrimination, which in turn can be used for the rejection of scintillations that are caused by scattered γ-rays or to discriminate noise. In Fig. 1 we present the principle of photon-counting gamma-camera imaging using our CCD-based gamma camera: the ultra gamma camera (UGC). The figure illustrates the case when a line pattern is imaged.

In gamma-camera imaging, photon counting is not only desirable for energy discrimination, but also 1) for suppressing noise

Manuscript received June 30, 2004. This work was supported by The Netherlands Organization for Scientific Research (NWO) under Grant 917.36.335.

G. A. de Vree, F. van der Have, and F. J. Beekman are with the Department of Nuclear Medicine, Image Sciences Institute and the Department of Pharmacology and Anatomy, Rudolf Magnus Institute of Neuroscience, University Medical Center Utrecht, 3584 CG, The Netherlands (e-mail: gerralt@isi.uu.nl).

A. H. Westra and K. M. Ligtvoet are with the Department of Medical Technology, University Medical Center, Utrecht 3584 CG, The Netherlands.

I. Moody is with the E2V Technologies, Chelmsford Essex CM1 2QU, U.K.

Digital Object Identifier 10.1109/TNS.2005.851443

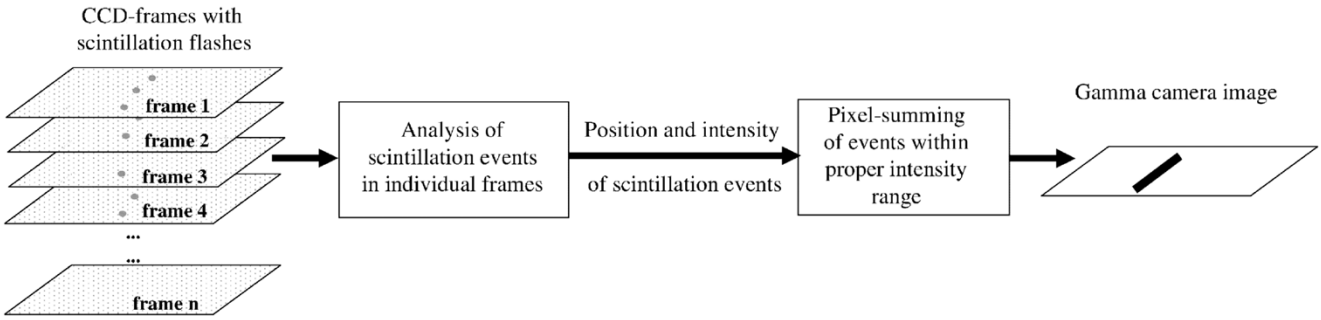

Fig. 1. Principle of photon counting in the CCD-based gamma camera in the case a line pattern on the scintillator is imaged: if the frame rate is high enough, each frame contains very few light clouds, which decreases the probability of overlap. In addition, the short time in which each frame is recorded reduces dark current noise accumulation, so the individual scintillation flashes can be distinguished better from the background.

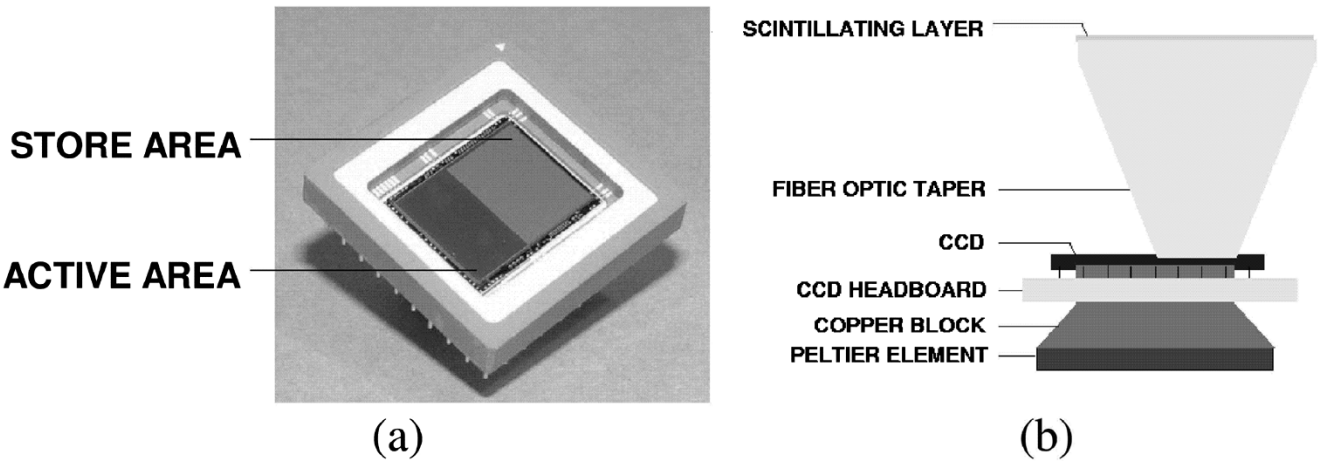

Fig. 2. EMCCD chip with (a) store area and active (photosensitive) area and (b) a possible set-up of a compact EMCCD-based gamma camera. The fiber optic taper can be used to increase the effective detector area per CCD and enables close packing of detector surfaces. A Peltier element can be used to cool the CCD chip in order to reduce the dark noise.

in the estimated number of detected gamma-rays and 2) for improving spatial resolution.

1) The estimated number of detected gamma quanta varies due to the varying number of light photons detected from each scintillation; the number of light photons per scintillation that reach a pixel varies because the light yield differs for each event and because the light spreads differently at different positions in a scintillation crystal. In addition, the dark current noise and readout noise introduce an extra variation in the detected signal per scintillation event. As a result, the estimate of the number of gamma interactions based on the amount of detected light can become quite inaccurate when integrating imaging systems instead of photon-counting systems are used. Furthermore, if the number of gamma photons in integrating systems is low, the dark noise build-up over the integration period will approach the light signal from a scintillation flash. When the CCD can be read out at a high frame rate in a photon-counting system such as proposed in Fig. 1, the light flashes can be detected before too much dark noise has accumulated.
2) Spatial resolution improvements may be obtained from photon counting by estimating the center of gravity of each light flash. This may help to improve the resolution limit of the gamma camera over the resolution as is set by the light spread in the scintillator and optical coupling.

When CCDs are used for reading out scintillation events they should have both a sufficiently high quantum efficiency and low dark current noise. Several CCDs with these properties are available. However, when these CCDs are operated at sufficiently high frame rates for photon-counting gamma-camera imaging, the readout noise becomes too high. A solution to this problem is to use an electron-multiplying CCD (EMCCD) such as that introduced in 2001 by E2V Technologies, Essex, U.K., and Texas Instruments. EMCCDs have extremely low readout noise, even at high readout speed (readout noise below 1 electron/pixel/readout at 11 MHz whereas the best conventional CCDs have a readout noise in the range of 10 to 100 electron/pixel/readout). Therefore, even at high frame rates, the total noise of an EMCCD can be very low with only moderate cooling of the CCD and without the need for an image intensifier [21]–[25].

In this paper we present a compact high-resolution photon-counting gamma camera based on an EMCCD, the UGC. A set-up of the UGC with scintillator and EMCCD is shown in Fig. 2. The main goal of the present paper is to describe the developed drive- and readout electronics and associated software for photon detection used in the UGC and to show some initial results of ultra-high-resolution gamma-ray imaging. On-board digital signal processing is presented as well.

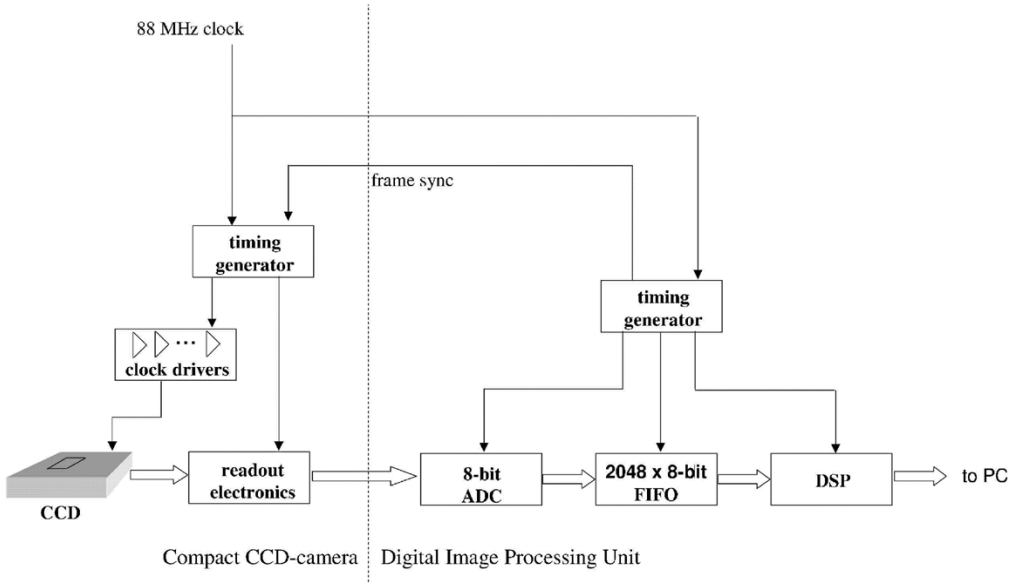

Fig. 3. Block diagram of the electronics of the UGC.

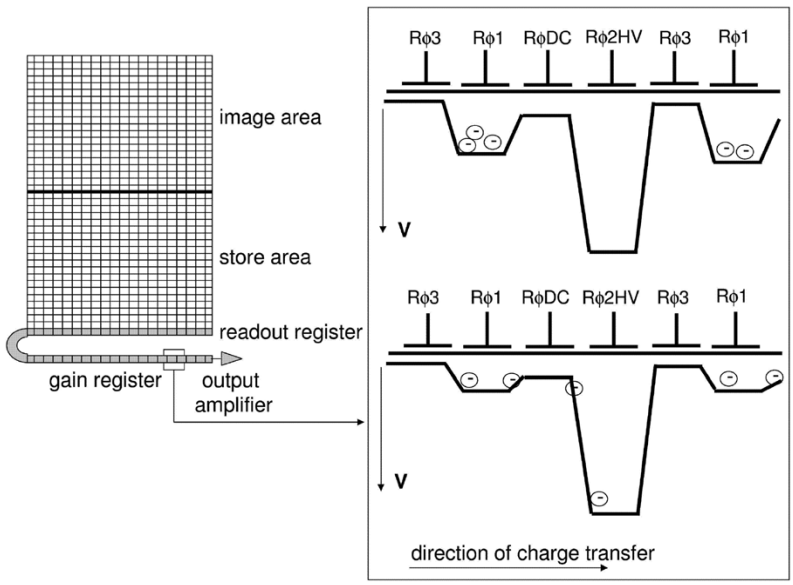

Fig. 4. Schematic diagram of an EMCCD showing the extra gain register and the multiplication by impact ionization in the gain register. The $\mathrm{R}\phi 2$ electrode of the conventional readout register is replaced by a dc electrode and an $\mathrm{R}\phi$2HV electrode in the gain register.

II. Materials and Methods

The electronics of the UGC includes the following:

1) an EMCCD;
2) clock drivers for driving the EMCCD;
3) analog readout electronics;
4) an analog–digital (A/D) converter;
5) a first-in first-out (FIFO) buffer;
6) a digital signal processor (DSP)-board for image processing and photon counting and for sending the detected locations and intensities to a personal computer (PC).

Two field programmable gate array (FPGA) based timing generators generate the digital timing clocks for the CCD and the digital logic components. A block diagram of the system is shown in Fig. 3. The first three parts together form a compact CCD camera, the last three parts form a digital image processing unit. The CCD camera is connected to the A/D converter in the digital image processing unit via a coaxial cable. This allows the digital image processing to be separated from the camera electronics and saves space in the camera. Furthermore it is possible to process the output of multiple CCD cameras with a single digital image processing unit.

A. Electron-Multiplying CCD

An EMCCD has a conventional CCD architecture except for an electron-multiplication structure (the gain register—see Fig. 4) that is inserted between the end of the readout register and the output amplifier. The gain register is similar to the readout register, except that one of the three phases is replaced by two electrodes, the first held at a fixed potential (dc) and the second clocked as normal but with a higher voltage amplitude

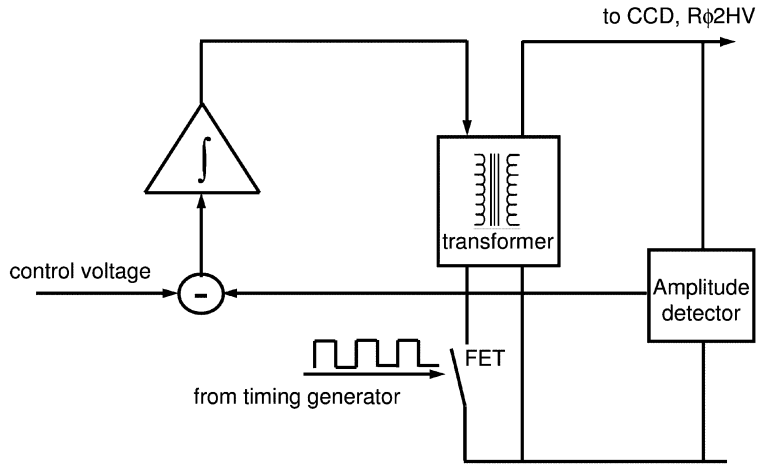

Fig. 5. Block diagram of the multiplication clock driver.

(between 40 V and 50 V; see Fig. 4). This combination of a fixed voltage electrode and a clocked electrode, with the relatively large difference between them, results in a high electric field. Due to this high electric field, electrons that are transferred through the gain register can experience avalanche multiplication (or impact ionization), which increases the number of electrons per charge packet and provides gain (see Fig. 4). The multiplication per transfer is quite small; only a factor of around 1.01 to 1.015, but when executed over a large number of transfers, a substantial gain is achieved. For example, with a multiplication factor of 1.015 per transfer over 591 transfers (in the case of the CCD65), a gain of 6630 is achieved.

When conventional CCDs are operated at high frame rates and cooled thermoelectrically to reduce the dark noise, the readout noise from the output amplifier is usually the main source of noise. Since the readout noise is independent of the signal level, the insertion of the electron amplification before the output amplifier (see Fig. 4) may increase the signal in the EMCCD above the readout noise, effectively reducing the readout noise. Therefore both the readout noise and the dark noise in a cooled EMCCD operating at high gain and high frame rate are very low. This causes a third noise source to become significant: the clock induced charge [(CIC), sometimes called spurious charge or transfer induced charge]. The CIC can be minimized by 1) making the parallel transfer frequency as large as possible (up to the maximum specified in the datasheet), 2) making the clock rise and fall times not too short, and 3) using reduced clocking amplitudes. The next section describes how clock drivers can be implemented to minimize CIC.

EMCCDs are available from E2V Technologies as L3Vision CCDs and from Texas Instruments as Impactron CCDs. The EMCCD used in the present work is a nonantibloomed (100% fill-factor) CCD65 from E2V Technologies. The CCD65 is a front-illuminated device with 288 lines and 576 pixels per line. The active area is 11.52 mm $\times$ 8.64 mm (20 μm $\times$ 30 μm pixel size) and the device operates in inverted-mode [(IMO), multiphase pinned (MPP)] in order to keep dark current low. For our application, the CCD has been equipped with a 3 mm fiber optic window, which is coupled in very close proximity of the CCD with optical cement. On top of this window, scintillators can be easily and efficiently coupled.

B. CCD Clock Drivers

Most of the drive electronics of the EMCCD are similar to the drive electronics of a conventional CCD. Digital electronics are used to generate the necessary clock sequences and level shifting buffers convert the digital clock sequences to the levels required by the CCD. However a significant difference between driving a conventional CCD and driving an EMCCD is that a higher voltage multiplication clock is required for the gain.

The high voltage multiplication clock of the L3Vision CCD requires voltages of up to 45 V in order to obtain a gain of around 1000$\times$ in the multiplication register. Conventional pulse buffers, with fast edges, would lead to significant power dissipation, both on and off the CCD, and might also cause dangerous clock overshoots that could damage the CCD. The total clock power can be calculated using $P = CV^2f$, at around 2 W. For fast clock edges of a few nanoseconds, the on-CCD power can approach 1 W, which is very undesirable. Better efficiency is achieved by using a resonant circuit with sine wave shape, resulting in an on-CCD power below 100 mW. Fig. 5 shows a block diagram of the multiplication clock driver as used inhere. A field effect transistor (FET) drives the primary winding of a transformer, the timing being determined by a logic level input. The power supply is derived from a summing integrator, one input setting the output level, and the other providing feedback from an amplitude detector connected to the HV output. Capacitors were adjusted to obtain resonance dependent upon printed circuit board (PCB) layout, with the CCD in circuit. The timing of the input pulse was then adjusted to give the correct relationship between the clocks, as defined in the CCD65 datasheet.

For buffering and level shifting the image and store clocks, we used the EL7457 chip from Elantec. In order to keep the CIC noise as low as possible, a series resistance was added at each output of the EL7457 chip to optimize the rise and fall times of the image and store clocks. Rise and fall times of approximately 200 ns were used, as recommended by E2V Technologies [26]. Pulse amplitudes were kept to the minimum required to transfer charge without smear, and were initially set at the typical values of -5 and $+7$ V. For the readout and gain register clock buffers ($\mathrm{R}\phi 1, \mathrm{R}\phi 2$, and $\mathrm{R}\phi 3$) and the charge detection node reset clock (see Figs. 3, and 4), we similarly used another driver chip from Elantec—the EL7156.

C. Analog Readout Electronics

The format of the output signal of an EMCCD is the same as the format of a conventional CCD. Therefore a standard CCD-processor (Sony CXA1310AQ) was used to perform correlated double sampling (CDS) and to add line-, field- and frame-synchronization patterns to the video signal. The standard analog video signal (CCIR) obtained this way can be directly viewed on a TV for debugging purposes or digitized and processed in the image processing unit.

D. DSP for Image Processing

For real-time photon counting, the analog video signal is digitized with a high-speed A/D converter and analyzed using a DSP. We used the fastest DSP Starter Kit (DSK) from Texas Instruments that is available—the DSK6416. It is based on the TMS320C6416 fixed point DSP. An input board containing the A/D converter, a FIFO-buffer and an FPGA-based timing generator is connected to the DSK via the DSK's expansion port connectors. The timing generator provides the sample clocks for the A/D converter, the timing for the FIFO buffer, and an interrupt signal for the DSP to start the direct memory access (DMA)-transfer of a block of pixel values from the FIFO-buffers into the SDRAM memory on the DSP board. The timing generator therefore is synchronized to the timing generator in the camera (frame sync; see block diagram in Fig. 3).

The photon-counting algorithm (see Section II-F) runs on the DSP and reads the images from the external SDRAM memory, transferring them to the internal DSP memory in blocks of 576 pixels (one line of a CCD-image). This is done with DMA-transfers, one block being processed while the next block is transferred to the internal memory. The results of the photon-counting algorithm (position and intensity of the detected scintillation light flashes) are sent to a PC via a USB connection on the DSK.

E. Implementation

For multipinhole SPECT imaging it is desirable that the gamma detectors are compact, such that one can put many detectors around an object to increase the sensitivity of the system [3], [8]. Therefore we developed a compact CCD headboard (4 cm × 4 cm). The headboard only contains the CCD and some decoupling capacitors. Via a 50 pin high-density connector, it is connected to a second board. This second board contains the drive electronics and the readout electronics for converting the CCD output into an analog video signal. A coaxial cable is used to connect the analog video signal to an A/D converter on the digital image processing board. A picture of the headboard with the CCD and the board with drive- and readout electronics is shown in Fig. 6.

In order to achieve high sensitivity and low noise, the EMCCD is thermoelectrically cooled down to −30 °C by using a water-cooled Peltier element. This almost totally eliminates the dark noise; this is of particular importance for the imaging of low energy isotopes (e.g., I-125, 27–35 keV) or in the presence of light loss due to strong fiber optic tapering.

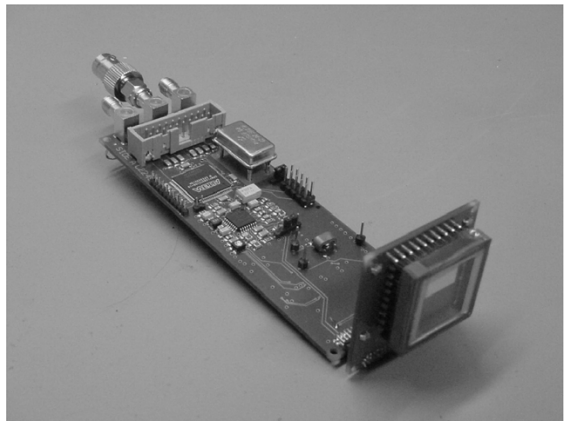

Fig. 6. Prototype of the newly developed PCBs for the compact EMCCD-based gamma camera.

F. Photon-Counting Algorithm

An efficient photon-counting algorithm is implemented in the DSP software in order to detect and localize scintillation events in real-time (50 images per second). One can set upper and lower limits for the intensity to distinguish scintillation events from background noise and disturbances like the direct interaction of gamma photons in the CCD.

The algorithm works as follows: each measurement starts with a background measurement in which the average (A) of the background signal is calculated for each pixel from 3000 images (1 minute measurement with no radioactivity). After the background measurement is finished, the gamma camera imaging can be started. Each CCD image (I_{ccd}) is first background corrected by subtracting the average background image A

$$I_{\mathrm{bg\cdot corr.}} = I_{\mathrm{ccd}} - A. \tag{1}$$

The background-corrected image $(I_{\mathrm{bg\cdot corr.}})$ is then smoothed with a 2-D Gaussian kernel (G; FWHM of 0.15 mm) to suppress high frequency noise in the image

$$I_{\mathrm{smoothed}} = I_{\mathrm{bg\cdot corr.}} * *G \tag{2}$$

where $**$ denotes a 2-D convolution. To increase speed, the convolution is implemented as two orthogonal one-dimensional Gaussian convolutions, which is mathematically identical to a single 2-D convolution because of the separability of the Gaussian convolution operation. In this filtered image (I_{smoothed}), scintillation events will appear as bright regions. If the value of a local maximum in I_{smoothed} lies between the lower limit ll and the upper limit ul, it is assumed to be a relevant scintillation event and its position and intensity are sent to the PC. In Section III some example images illustrating the algorithm are shown and discussed.

III. Experimental Results

Fig. 7 shows some images of the photon-counting algorithm at work. An area on the CCD with a size of 2 mm × 2 mm is shown. Fig. 7(a) shows a raw CCD image I_{ccd}, and Fig. 7(b) shows the average background image A. Fig. 7(c) shows the CCD image minus the average background image $I_{\mathrm{bg\cdot corr.}}$.

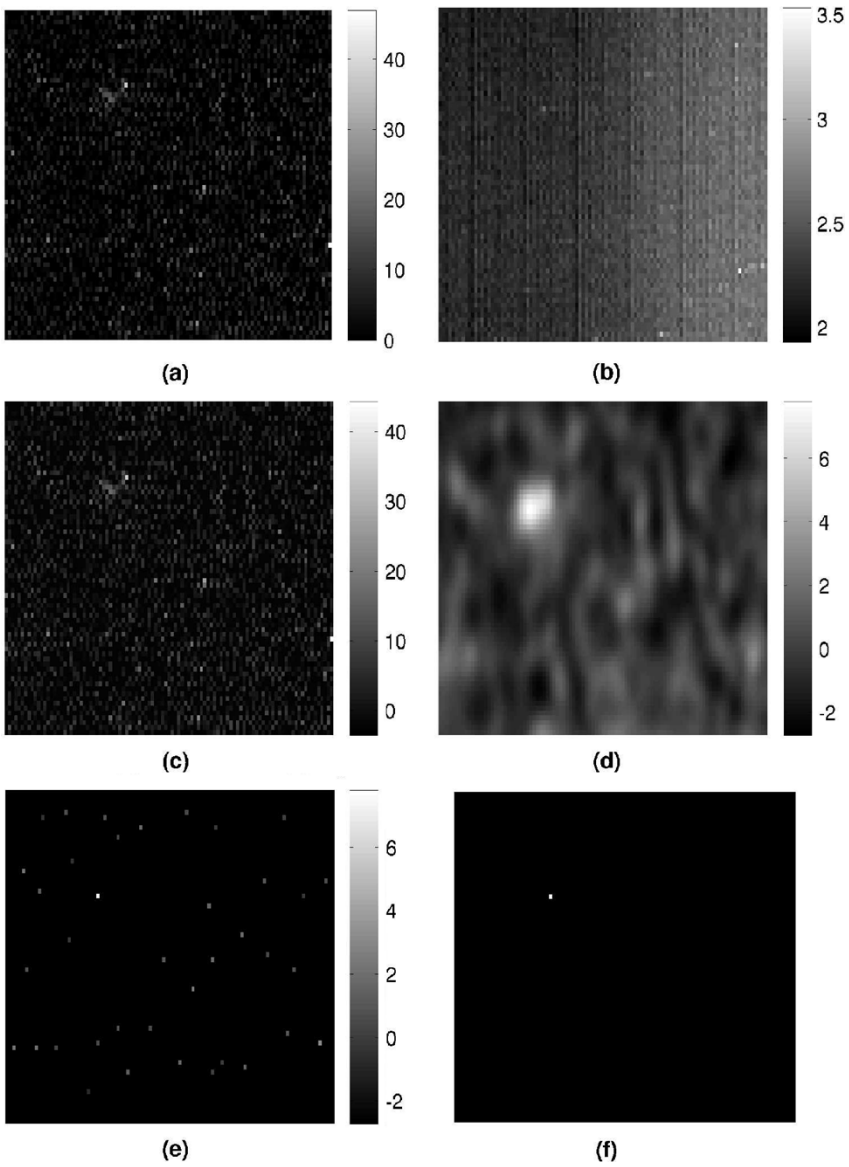

Fig. 7. Images illustrating the algorithm at work, showing 2 mm × 2 mm CCD-area. (a) Raw CCD image: I_{ccd}. (b) Average background image: A. (c) Frame (a) minus Frame (b): $I_{\mathrm{bg.corr.}}$. (d) Frame (c) after smoothing: I_{smoothed}. (e) Local maxima in I_{smoothed} of Frame (d). (f) Position of detected scintillation event.

Fig. 7(d) shows the same image after smoothing I_{smoothed}), which provides blobs with different intensities that can be used for localizing the events. In Fig. 7(e) the local maxima provided by the blobs in I_{smoothed} as well as their differing intensities represented by different grey values are shown. Fig. 7(f) shows the remaining event locations after intensity discrimination: only one local maximum has a value between the lower limit and the upper limit, and therefore only one scintillation event is detected in this image.

To evaluate the spectral capabilities of the UGC, the camera was flood irradiated with a gamma-source and a histogram of the detected flash intensities was plotted from the listmode output (i.e., the detected energy spectrum). This experiment was carried out both with Co-57 (122 keV) and with I-129 (30 keV). The results are shown in Fig. 8. A well-defined single peak is seen both for Co-57 and for I-129. Energy resolutions of 40 keV and 42 keV FWHM are estimated from the Co-57 spectrum and the I-129 spectrum, respectively.

To determine spatial resolution, line pattern images with the camera were acquired using the set-up as shown in Fig. 9(a). Two lead blocks separated by a narrow slit (50 μm wide) were used to project a line pattern from a Co-57 radioactive source (122 keV; 4 MBq; 3 mm diameter) onto a 1 mm thick micro-columnar scintillator (CsI(Tl) FOS from Hamamatsu). The use of a slit formed by two lead blocks is a standard method to measure the intrinsic resolution of clinical gamma cameras. Since the CCD has a nonsquare pixel size (20 μm × 30 μm), the resolution has been measured for two orthogonal directions: the slit approximately parallel to the CCD-columns and the slit approximately parallel to the CCD-lines. The energy-discrimination settings (lower-limitll and upper-limit ul) for the photon-counting algorithm in the DSP were set very wide, with only a lower-limitll to exclude most of the noise. Further energy discrimination was done in the PC after the measurements were finished, by selecting only those events from the listmode data that were in the valid energy range.

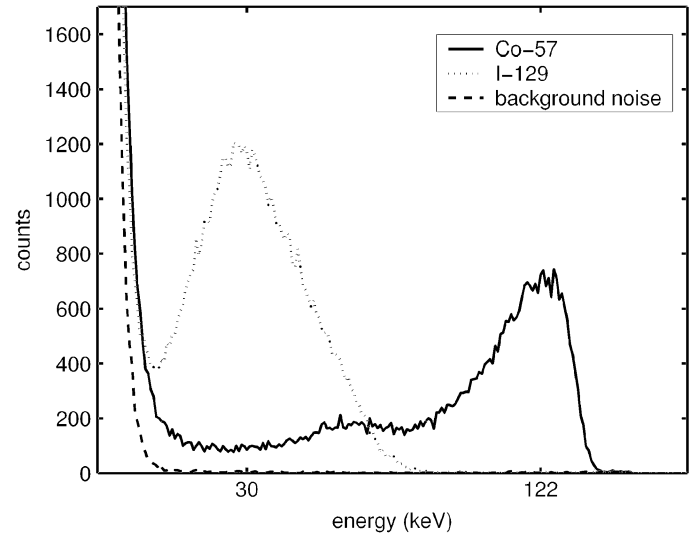

Fig. 8. Detected energy spectrum for Co-57 (solid line) and for I-129 (dotted line). A measurement without activity is also shown (dashed line) to illustrate the difference between the scintillation signal and the background and CCD noise.

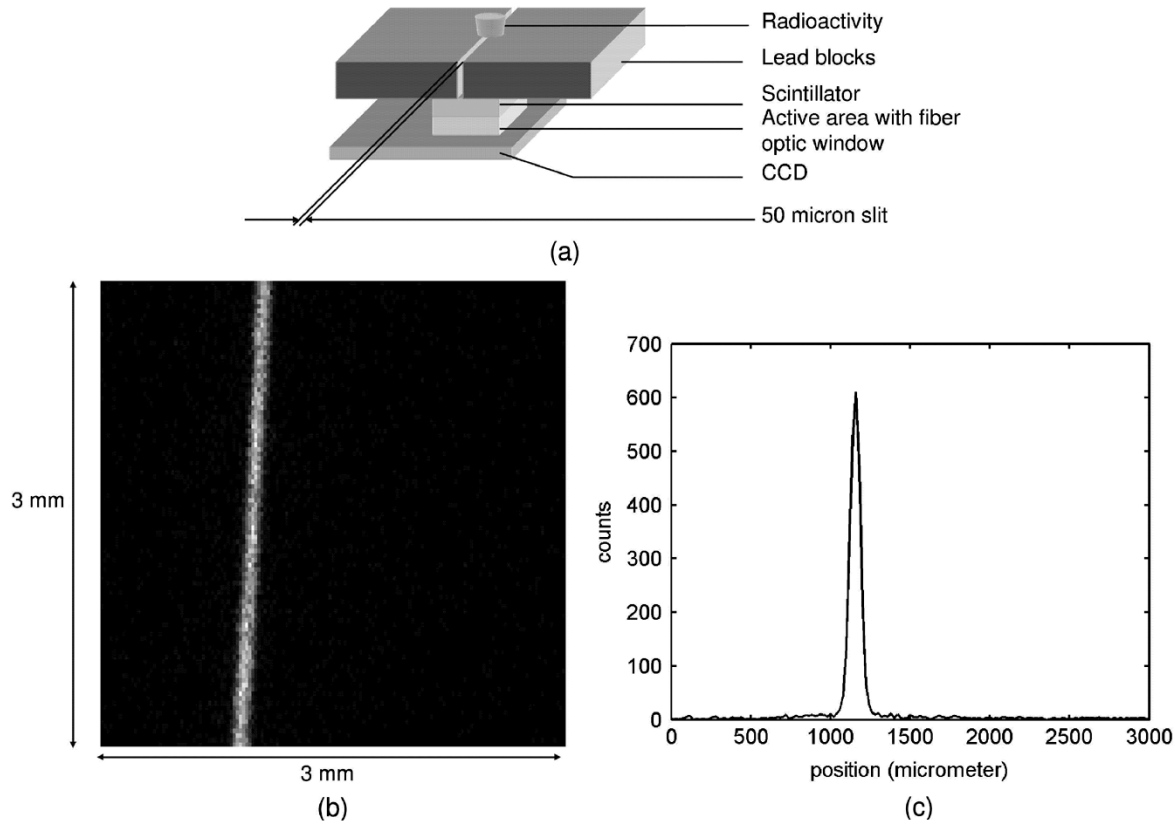

Fig. 9. Resolution measurement: (a) measurement setup, (b) resulting image, and (c) image intensity profile.

In Fig. 9(b) and (c), the resulting gamma-camera image and a profile over 1 mm perpendicular to the line pattern are shown for the case that the slit is parallel to the CCD-columns. An FWHM line width of 77 μm was measured from the profile. Corrected for the beam width of 50 μm, this gives a spatial resolution in the direction parallel to the CCD-lines of approximately 60 μm FWHM. The resolution measurement in the perpendicular direction (slit parallel to the CCD-lines) results in an FWHM line-width of 108 μm. After correcting for the beam width, this gives a FWHM resolution of 96 μm in the column-direction. The difference in x and y resolution may be caused by the different pixel lengths in the x and y direction.

IV. Conclusion and Discussion

We developed an EMCCD-based compact gamma camera with ultra-high spatial resolution and the ability to perform energy discrimination. The camera operates at 50 images per

second and with the presented DSP hardware and software it is able to do real-time photon counting. Using dedicated electronics and algorithms, we were able to reach an intrinsic spatial resolution as good as 60 μm FWHM. The resolution is degraded in the direction where the pixel length is longer, which indicates that a better resolution may be achieved when smaller CCD pixels are used. The frame rate of the camera is high enough to limit dark current noise build-up and it enables a maximum count rate that is more than sufficient for small animal SPECT. For example, in the U-SPECT-I system [9] during a typical small animal data acquisition, less than one gamma photon per second per cm^2 is incident on the detector during normal operation, which means that in that case most of the CCD-images will not be illuminated by scintillation events and therefore the probability of overlapping scintillation events is negligible.

For the present system a fast algorithm for scintillation detection was implemented in the DSP. This algorithm does not take into account all statistical properties of the dark current and the scintillation signal. In the future the performance of the camera may be improved by the use of statistical detection approaches. This will require an efficient implementation to preserve real-time processing.

First experiments demonstrate that the described electronics and event processing are able to do efficient real-time photon counting including energy discrimination. In future work we intend to investigate how the developed gamma camera can be optimized for the imaging of other isotopes and gamma energies, and to investigate effects of different scintillators and fiber optic tapering or other means of optical coupling.

The relatively thin columnar crystal layer (1 mm) used in the present work is adequate to secure the required detection yield for lower photon energies and prevents light spreading. Higher energy photons though, such as those emitted by radionuclides like Tc-99 m (140 keV), have a low probability of interaction with such thin crystals. Longer columnar crystals are under development at several companies. However, in the case of pinhole collimation, a "parallax" error would remain, since for offset source positions the radiation penetrates into the columns at an angle, and therefore the column in which the interaction will take place cannot be determined *a priori*. Consequently, different columns will scintillate when gammas are emitted from a single point. This will result in an undesirable line pattern instead of a well-defined point-like emission of light at the interface between the crystal and the CCD. We have proposed to avoid this problem by directing the fibers toward the pinhole ("cone beam crystals"). Using such crystals, the scintillation light is transmitted along the same direction as the direction traveled by the gamma quantum. As a result, the depth-of-interaction in the scintillator will not influence the place where the light hits the CCD [8].

The resulting detector may help to bring about significant improvements in radio-molecular imaging.

ACKNOWLEDGMENT

The authors would like to thank B. Altorffer and H. Essers of the Department of Medical Technology (MeT) of the University Medical Center (UMC), Utrecht, The Netherlands, for their technical assistance. The authors would also like to thank colleague B. Vastenhouw for fruitful discussions.

REFERENCES

[1] P. D. Acton and H. F. Kung, "Small animal imaging with high resolution single photon emission tomography," *Nucl. Med. Biol.*, vol. 30, no. 8, pp. 889–895, Nov. 2003.

[2] M. A. King, T. H. Pretorius, T. Farncombe, and F. J. Beekman, "Introduction to the physics of molecular imaging with radioactive tracers in small animals," *J. Cell. Biochem.*, vol. 87, no. S39, pp. 221–230, 2002.

[3] R. K. Rowe, J. N. Aarsvold, H. H. Barrett, J. C. Chen, W. P. Klein, B. A. Moore, I. W. Pang, D. D. Patton, and T. A. White, "A stationary hemispherical SPECT imager for three-dimensional brain imaging," *J. Nucl. Med.*, vol. 34, pp. 474–480, Mar. 1993.

[4] F. J. Beekman, A. P. Colijn, B. Vastenhouw, V. M. Wiegant, and M. A. F. M. Gerrits, "High-resolution emission tomography of small laboratory animals: Physics and gamma-astronomy meet molecular biology," *Nucl. Instrum. Methods Phys. Res. A*, vol. 509, pp. 229–234, Aug. 2003.

[5] G. A. Kastis, H. B. Barber, H. H. Barrett, H. C. Gifford, I. W. Pang, D. D. Patton, G. Stevenson, and D. W. Wilson, "High resolution SPECT imager for three-dimensional imaging of small animals," *J. Nucl. Med.*, vol. 39, p. 9P, 1998. (abstract).

[6] Z. Liu, G. A. Kastis, G. D. Stevenson, H. H. Barrett, L. R. Furenlid, M. A. Kupinski, D. D. Patton, and D. W. Wilson, "Quantative analysis of acute myocardial infarct in rat hearts with ischemia-reperfusion using a high-resolution stationary SPECT system," *J. Nucl. Med.*, vol. 43, pp. 474–480, Jul. 2002.

[7] N. U. Schramm, G. Ebel, U. Engeland, T. Schurrat, M. Béhé, and T. M. Behr, "High-resolution SPECT using multipinhole collimation," *IEEE Trans. Nucl. Sci.*, vol. 50, no. 3, pp. 315–320, Jun. 2003.

[8] F. J. Beekman and B. Vastenhouw, "Design and simulation of a high-resolution stationary SPECT system for small animals," *Phys. Med. Biol.*, vol. 49, pp. 4579–4592, 2004.

[9] F. J. Beekman, F. van der Have, B. Vastenhouw, A. J. A. van der Linden, P. P. van Rijk, J. P. H. Burbach, and M. P. Smidt, "U-SPECT I: A novel system for submillimeter-resolution tomography with radiolabeled molecules in mice," *J. Nucl. Med.*, vol. 46, pp. 1194–1200, 2005.

[10] R. F. Brem, J. M. Schoonjans, D. A. Kieper, S. Majewski, S. Goodman, and C. Civelek, "High-resolution scintimammography: A pilot study," *J. Nucl. Med.*, vol. 43, no. 7, pp. 909–915, Jul. 2002.

[11] D. P. McElroy, E. J. Hoffman, L. MacDonald, B. E. Patt, J. S. Iwanczyk, Y. Yamaguchi, and C. S. Levin, "Evaluation of breast tumor detectability with two dedicated, compact scintillation cameras," *IEEE Trans. Nucl. Sci.*, pt. 1, vol. 49, no. 3, pp. 794–802, Jun. 2002.

[12] F. J. Beekman, D. P. McElroy, F. Berger, S. S. Gambhir, E. J. Hoffman, and S. R. Cherry, "Toward in vivo nuclear microscopy; I-125 imaging in mice using micro-pinholes," *Eur. J. Nucl. Med.*, vol. 29, no. 7, pp. 933–938, Jul. 2002.

[13] O. Gal, F. Jean, F. Lainé, and C. Lévêque, "The CARTOGAM portable gamma imaging system," *IEEE Trans. Nucl. Sci.*, pt. 2, vol. 47, no. 3, pp. 952–956, Jun. 2000.

[14] L. Menard, Y. Charon, M. Solal, P. Laniece, R. Mastrippolito, L. Pinot, L. Ploux, M. Ricard, and L. Valentin, "POCI: A compact high resolution gamma camera for intra-operative surgical use," *IEEE Trans. Nucl. Sci.*, vol. 45, no. 3, pp. 1293–1297, Jun. 1998.

[15] Y. Charon, P. Laniece, and H. Tricoire, "Radio-imaging for quantitative autoradiography in biology," *Nucl. Med. Biol.*, vol. 25, no. 8, pp. 699–704, Nov. 1998.

[16] J. L. Matteson, W. Coburn, F. Duttweiler, W. A. Heindl, G. L. Huszar, P. C. Leblanc, M. R. Pelling, L. E. Peterson, R. E. Rothschild, R. T. Skelton, P. L. Hink, and C. Crabtree, "CdZnTe arrays for astrophysics applications," in *Proc. SPIE*, vol. 3115, Jul. 1997, pp. 160–175.

[17] H. B. Barber, "Applications of semiconductor detectors to nuclear medicine," *Nucl. Instrum. Methods Phys. Res. A*, vol. 436, pp. 102–110, Oct. 1999.

[18] X. Llopart, M. Campbell, R. Dinapoli, D. S. Segundo, and E. Pemigotti, "Medipix2: A 64-k pixel readout chip with 55 μm square elements working in single photon counting mode," *IEEE Trans. Nucl. Sci.*, vol. 49, no. 5, pp. 2279–2283, Oct. 2002.

[19] Z. He, W. Li, G. F. Knoll, D. K. Wehe, J. Berry, and C. M. Stahle, "3-D position sensitive CdZnTe gamma-ray spectrometers," *Nucl. Instrum. Methods Phys. Res. A*, vol. 422, pp. 173–178, 1999.

[20] V. Nagarkar, J. S. Gordon, S. Vasile, P. Gothoskar, and F. Hopkins, "High resolution X-Ray sensor for non destructive evaluation," *IEEE Trans. Nucl. Sci.*, vol. 43, no. 3, pp. 1559–1563, Jun. 1996.

[21] P. Jerram, P. Pool, R. Bell, D. Burt, S. Bowring, S. Spencer, M. Hazelwood, I. Moody, N. Catlett, and P. Heyes, "The LLLCCD: Low light imaging without the need for an intensifier," in *Proc. SPIE*, vol. 4306, 2001, pp. 178–186.

[22] M. S. Robbins and B. J. Hadwen, "The noise performance of electron multiplying charge-coupled devices," *IEEE Trans. Electron Devices*, vol. 50, no. 5, pp. 1227–1232, May 2003.

[23] C. D. Mackay, R. N. Tubbs, R. Bell, D. Burt, and I. Moody, "Sub-electron read noise at MHz pixel rates," in *Proc. SPIE*, vol. 4306, 2001, pp. 289–298.

[24] J. Hynecek, "Impactron—A new solid state image intensifier," *IEEE Trans. Electron Devices*, vol. 48, no. 10, pp. 2238–2241, Oct. 2001.

[25] D. J. Denvir and E. Conroy, "Electron-multiplying CCD: The new ICCD," in *Proc. SPIE*, vol. 4796, Feb. 2003, pp. 164–174.

[26] Low-Light Technical Note 4, Dark Signal and Clock-Induced Charge in L3Vision CCD Sensors, E2V Technologies, Essex, U.K. [Online]. Available: http://e2vtechnologies.com